


Evidence of Three-Dimensional Asymmetries Seeded by High-Density Carbon-Ablator Nonuniformity in Experiments at the National Ignition Facility

D. T. Casey,¹ B. J. MacGowan,¹ J. D. Sater,¹ A. B. Zylstra,¹ O. L. Landen,¹ J. Milovich,¹ O. A. Hurricane,¹ A. L. Kritcher,¹ M. Hohenberger,¹ K. Baker,¹ S. Le Pape,¹ T. Döppner,¹ C. Weber,¹ H. Huang,² C. Kong,² J. Biener,¹ C. V. Young,¹ S. Haan,¹ R. C. Nora,¹ S. Ross,¹ H. Robey,¹ M. Stadermann,¹ A. Nikroo,¹ D. A. Callahan,¹ R. M. Bionta,¹ K. D. Hahn,¹ A. S. Moore,¹ D. Schlossberg,¹ M. Bruhn,¹ K. Sequoia,² N. Rice,² M. Farrell,² and C. Wild³

¹Lawrence Livermore National Laboratory, Livermore, California 94550, USA

²General Atomics, San Diego, California 92186, USA

³Diamond Materials, 79108 Freiburg, Germany

 (Received 4 August 2020; revised 22 October 2020; accepted 30 November 2020; published 12 January 2021)

Inertial confinement fusion implosions must achieve high in-flight shell velocity, sufficient energy coupling between the hot spot and imploding shell, and high areal density ($\rho R = \int \rho dr$) at stagnation. Asymmetries in ρR degrade the coupling of shell kinetic energy to the hot spot and reduce the confinement of that energy. We present the first evidence that nonuniformity in the ablator shell thickness ($\sim 0.5\%$ of the total thickness) in high-density carbon experiments is a significant cause for observed 3D ρR asymmetries at the National Ignition Facility. These shell-thickness nonuniformities have significantly impacted some recent experiments leading to ρR asymmetries on the order of $\sim 25\%$ of the average ρR and hot spot velocities of ~ 100 km/s. This work reveals the origin of a significant implosion performance degradation in ignition experiments and places stringent new requirements on capsule thickness metrology and symmetry.

DOI: [10.1103/PhysRevLett.126.025002](https://doi.org/10.1103/PhysRevLett.126.025002)

In inertial confinement fusion (ICF) experiments performed at the National Ignition Facility (NIF) [1], capsules of deuterium and tritium (DT) fuel are imploded to high densities and temperatures to initiate alpha-particle self-heating and fusion burn [2,3]. The indirect-drive ICF concept uses a laser to irradiate a high- Z cylindrical hohlraum, which attempts to produce a nearly uniform, quasithermal, x-ray drive. The x-ray drive then ablates the outer layers of the capsule, compressing the remaining ablator and an inner layer of cryogenically frozen DT radially inward. This imploding shell converges on and compresses a gaseous DT region to form a hot spot. To achieve ignition, the DT hot spot must have high enough energy density confined for an adequate time to spark hot spot self-heating and start a burn wave through the dense DT shell. This requirement can be equivalently expressed as a condition of $P\tau$, where P is the hot spot pressure, a measure of the energy density, and τ is the confinement time of that energy [4,5]. To produce high $P\tau$, an implosion must have high in-flight implosion velocity (v_{imp}), sufficient coupling between the in-flight shell and hot spot, and high areal density (or ρR defined as $\rho R = \int \rho dr$) at stagnation.

The coupling of the shell kinetic energy and the confinement of that energy are both degraded by three-dimensional (3D) ρR asymmetry. Recent analysis using a simplified two-piston system shows [6] that, in the limit of weak-alpha

heating, $(P\tau/P\tau_{\text{1D}}) \approx (1 - f^2)$ and $(Y/Y_{\text{1D}}) \approx (1 - f^2)^{10/3}$, where Y/Y_{1D} is the yield (Y) normalized by idealized 1D symmetric yield (Y_{1D}) and $f = [(\rho R_{\text{max}} - \rho R_{\text{min}})/(\rho R_{\text{max}} + \rho R_{\text{min}})] \approx (v_{\text{HS}}/v_{\text{imp}})$. Here ρR_{max} and ρR_{min} are the maximum and minimum areal densities of the dense shell, respectively; v_{HS} is the bulk velocity of the burning hot spot near peak convergence, and v_{imp} is the peak implosion velocity. These relationships reveal that a $\sim 25\%$ asymmetry in $\delta\rho R/\rho R$ (or an observed hot spot velocity $v_{\text{HS}} \sim 100$ km/s for an implosion velocity of $v_{\text{imp}} \sim 400$ km/s) can result in an $\sim 7\%$ loss in hot spot internal energy corresponding to an $\sim 22\%$ reduction in no-alpha yield. Furthermore, the impact of this degradation can be much larger if alpha heating is significant. For example, this level of asymmetry is predicted to result in an $\sim 38\%$ reduction in total yield, including estimates for alpha heating [7], for an implosion with an unperturbed neutron yield of 2×10^{16} and neutron down-scattered ratio [8–10] (or DSR, which is related to the $\rho R[\text{g/cm}^2] \sim 0.2\text{DSR}[\%]$) of $\text{DSR} = 3.3\%$, resulting in a yield of about 1.3×10^{16} . Experiments with intentional asymmetries [11,12] have shown yield degradations consistent with these arguments. Furthermore, trends over all experiments suggest low-mode asymmetries are among several important degradations in current ICF experiments at the NIF, as also recently shown with Compton radiography measurements [13].

Percent-level deviations from perfect radiation drive or target uniformity can seed asymmetries and cause them to grow during the implosion. This, in turn, reduces the hot spot-shell coupling and degrades confinement of that energy, resulting in reduced overall performance. In fact, experiments often exhibit signatures of asymmetry, and understanding their origin is of paramount importance in mitigating and removing their impact. Herein, we show new evidence that ablator shell-thickness nonuniformity is an important cause of observed low-mode asymmetries. When combined with other recent results [14] that identified the principal causes of radiation drive nonuniformity, this newly identified ablator thickness seed appears among the primary causes of 3D asymmetries.

The experiments described herein used 192 NIF laser beams to indirectly drive a range of 6.20–6.72-mm-diameter depleted uranium hohlraums, each with a thin Au coating. The laser beams enter through laser entrance holes (LEHs) at each end of the cylindrical hohlraum that ranged from 3.64 to 4 mm in diameter depending on the specific design details of each platform. In each experiment, the hohlraum was filled with helium gas between 0.3 and 0.45 mg/cc fill to tamp the hohlraum wall. Inside the hohlraum is a 55–65- μm -thick cryogenically frozen deuterium-tritium ice layer of density 0.255 g/cm³ inside a 1000–1100 μm inner radius high-density carbon (HDC) [15–27] capsule. The capsules used were between 76 and 80 μm thick, predominantly made of 3.45 g/cm³ microcrystalline or 3.33 g/cm³ nanocrystalline grains. The shells included a layer doped with W to $\sim 0.3\%$ – 0.4% atomic percent in a ~ 20 - μm -thick layer to shield the DT-ablator interface from hard x rays to maintain a favorable Atwood number reducing high-mode DT-ablator instability growth [28].

Efficient conversion of in-flight kinetic energy into hot spot internal energy requires keeping drive asymmetry limited to subpercent levels during the implosion. Recently, a study [14] revealed the role of x-ray drive radiation asymmetries resulting from peak laser power balance and diagnostic window losses as a principle cause of observed asymmetries [14,29]. Similar work in direct-drive implosions at the OMEGA laser facility have tied observed low-mode asymmetries to inducements by the drive from laser beam pointing and power or timing fluctuations [30,31]. Specifically with regard to the experiments at the NIF [14], roughly $\sim 75\%$ of select cases were explained by radiation nonuniformities, while $\sim 25\%$ appear to be dominated by some other unidentified mechanisms. Furthermore, several recent experiments seemed less likely to be explained by radiation asymmetries alone, motivating a search for other causes including the possibility of capsule inducements as described below.

To measure the HDC shell-thickness uniformity, several methods are employed. One places the capsule on a radiographic film plate and uses backlit x-ray radiography

(contact radiograph) [32,33]. This technique can also measure the concentricity of the inner and outer surfaces to ~ 0.15 μm and can view the capsule only from a single view at present, making it useful for detecting problem capsules and for performing overall batch surveillance. After the target is built and is undergoing preparations to be shot, the phase contrast enhanced x-ray radiography [34–36] technique is used to characterize the shell thickness in 3D in the “cryotarpos” layering and imaging station from three orthogonal views [36]. The HDC shell is viewed through the LEH along the hohlraum axis and through “starburst” cutouts at the hohlraum equator, or “side views,” as illustrated by Fig. 1(a). Figure 1(b) shows an x-ray radiograph from capsule KC461-03 that was used on experiment N181104 viewed from one of the side views, while Fig. 1(c) shows a radiograph along the LEH view. Figures 1(d) and 1(e) show the HDC shell Δ thickness (value minus the average) as a function of the angle along the image (where phase = 0 is the right-hand axis of the image and the angle increases counterclockwise from there). Fitting the available data results in an amplitude of $0.78 \pm 0.2\%$ out of an average thickness of 78 μm [37].

To build more confidence in the capsule thickness asymmetry measurements, the three orthogonal views from the cryotarpos layering station were fitted with a pure mode 1 and compared along their common axes for the capsules used in this dataset. Figure 2 shows the 90-150 components of the thickness mode 1 (where 90 is the polar angle in degrees and 150 is the azimuthal angle) from the LEH view compared to the side 1 view, the 90-60 component determined from the LEH and side 2 views, and the 0-0 component determined from the side 1 and side 2 views. The scatter in the data points is larger than the statistical uncertainty because of errors in the edge-finding routine used to identify the inner and outer surfaces and background issues not captured by statistical uncertainty of the data. The root-mean square (rms) of all available HDC data when comparing the two side views to LEH views is ~ 0.15 μm . Figure 2 also compares the side views to each other along the 0-0 direction, and the rms is ~ 0.3 μm . Because these values are larger than the statistical uncertainty, we take these comparisons to be representative of the total error in determining the mode-1 asymmetry of the capsule thickness including nonstatistical fluctuations from effects described earlier. Furthermore, the LEH data are more extensive and of generally higher quality, and so we infer the LEH view error is 0.1 μm and the side view error is 0.15 μm .

Two-dimensional simulations using the radiation hydrodynamics code HYDRA [38] can calculate the predicted impact of capsule thickness and, hence, ρR asymmetries on implosions like those observed here. Figure 3 shows the simulated hot spot velocity as a function of the capsule mode-1 amplitude (red circles) compared with simulations for an 1100 μm inner radius HDC capsule. For this particular HDC platform, the predicted sensitivity is

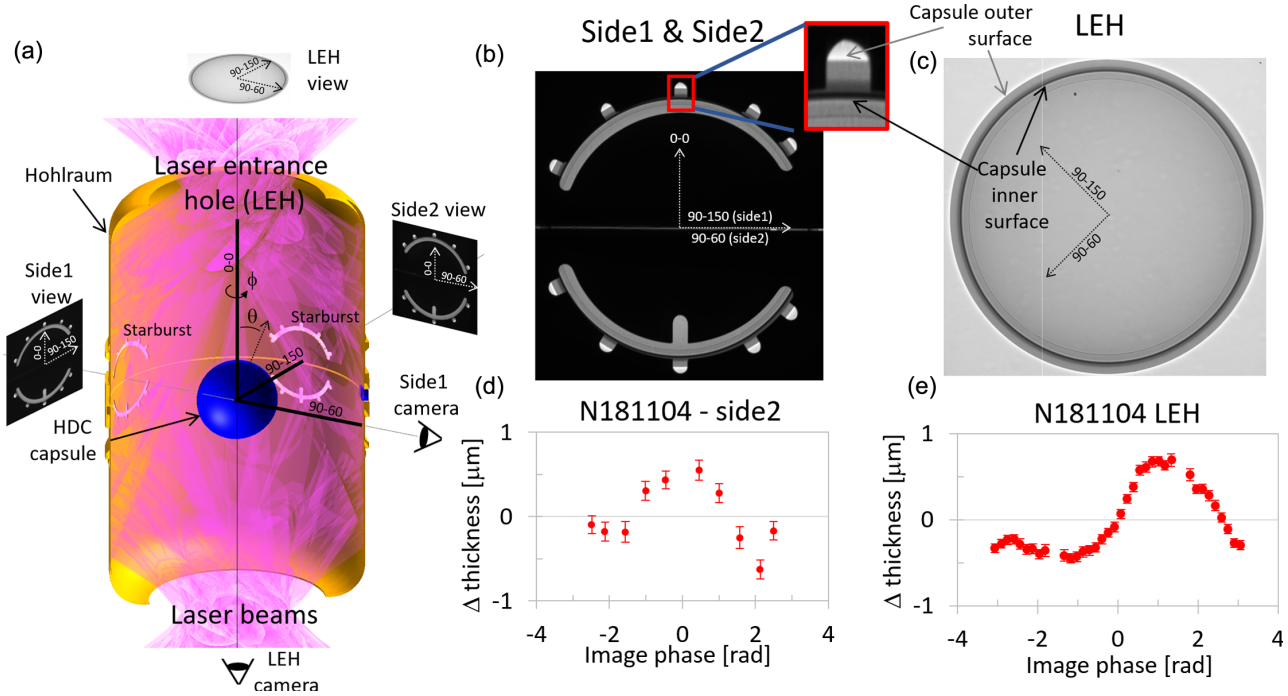


FIG. 1. (a) Schematic of hohlraum, capsule, and radiograph lines of sight. (b),(c) Radiograph measurements of the HDC capsule used on shot N181104 from the side and LEH views. (d),(e) HDC capsule thickness asymmetries measured from the radiographs in (b) and (c).

~ 110 km/s/%-ml (kilometer per second per percent mode 1), becoming nonlinear at high initial seed amplitude [39,40]. Figure 3 also shows the hot spot velocity sensitivity as a function of applied mode-1 flux asymmetries (opposite sign) in units of percent relative to the peak flux and applied over the entire pulse. The results are consistent with prior simulation studies of radiation-flux-induced asymmetries [41].

Interestingly, the sensitivity to flux and capsule thickness is about the same but with opposite phase. This phase

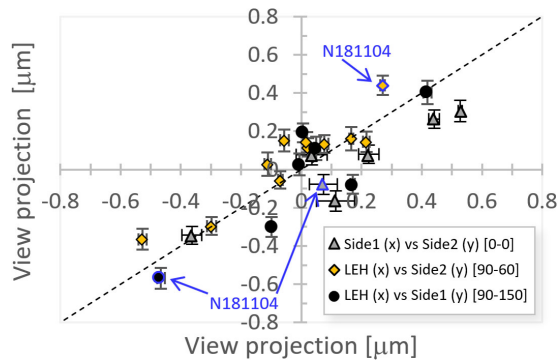


FIG. 2. A comparison between the 90–150 component of the capsule thickness mode 1 determined from the fit projections along the common 90–150 axis of the orthogonal LEH and side 1 radiographs (black circles), the 90–60 component from the LEH and side 2 radiographs along their common axis (orange diamonds), and the 0–0 component from the side 1 and side 2 data along their common axis (gray triangles).

difference is because the initially thicker capsule side implodes to a slower peak velocity than the thinner side, resulting in a delay in reaching peak convergence. This is shown by examining a first-order solution [42] (neglecting the effect of late time ablation pressure or “coast”) to the spherical rocket equations: $v_{\text{imp}} \sim 2\pi R_0^2 p_{\text{max}} t_{\text{off}} / M_0$, where R_0 is the initial capsule radius, p_{max} is the peak ablation pressure, t_{off} is the time of peak ablation pressure, and M_0 is the initial capsule and DT payload mass. When perturbed for small changes in the initial mass (dm_0/m_0), the change

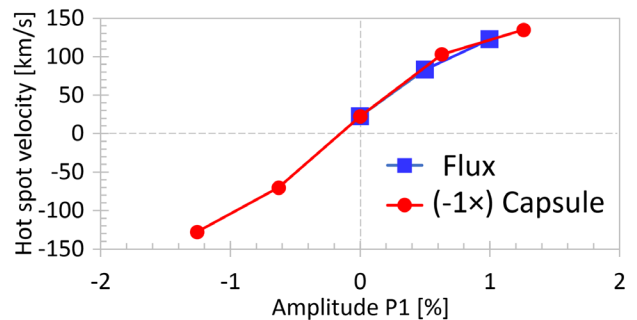


FIG. 3. Simulations of HDC capsule thickness-induced hot spot velocity versus the amplitude of the shell-thickness asymmetry (red circles) with an intentional sign change for easier comparison to the capsule radiation flux-induced hot spot velocity versus angle (blue squares). The simulations show that HDC thickness will drive a hot spot velocity very similarly to the previously identified capsule flux asymmetries [14,41].

in v_{imp} becomes $dv_{\text{imp}}/v_{\text{imp}} \sim -dm_0/m_0$. Therefore, somewhat counterintuitively, the initially thicker side will reach lower ρR because of spherical convergence as its implosion trajectory is delayed by the initially weaker acceleration. Then, as hot spot pressure builds, the lower ρR part of the shell is decelerated more than the higher ρR part, further amplifying the difference. The result is that by peak neutron production the resultant hot spot velocity becomes directed toward the lower ρR or the initially thicker side. This is the opposite direction of a flux (F) asymmetry (dF/F), which will typically drive the side of the capsule faster where the flux is higher like $dv_{\text{imp}}/v_{\text{imp}} \sim \frac{7}{8}dF/F$, where the $7/8$ comes from the relative sensitivity of flux and ablation pressure [43]. This predicts a net hot spot velocity directed away from the initially higher flux side. Note that numerical calculations are somewhat less sensitive ($\sim 30\%$) than these rough estimates but that the sensitivity and sign difference between flux and capsule mass asymmetry is preserved. Furthermore, simulations with HYDRA show that the presence of graded dopant can further reduce the sensitivity of outer surface perturbations, because the ablation rate stays higher longer as it must traverse more undoped material before reaching the doped layer on the initially thicker side where the ablation rate will drop. This ablation rate effect with doped layers helps explain why the sensitivities of flux perturbations and mass perturbations, as calculated, are nearly equal and opposite phase in Fig. 3.

Experiments often show evidence of significant ρR asymmetry and resultant hot spot velocity. Shot N181104 presents an interesting example as is not easily explained by drive and diagnostic window asymmetries and so is among the anomalous $\sim 25\%$ of cases [14]. Observations of the ρR asymmetry are made using the anisotropy of the emitted 14 MeV yield with the real time neutron activation detector suite (RTNADs), a more precise and larger activation detector suite to its predecessor FNADs [44]. The observed RTNAD data for N181104 is presented in Fig. 4 along with a $\ell \leq 2$ Y_{lm} -mode fit presented in NIF angular coordinates, theta and phi. The RTNAD data measure the unscattered neutron yield, which is sensitive to path integrated areal density (ρL) via neutron attenuation, where $Y/Y_{\text{avg}} \approx 1 - 0.2 \times \delta\rho L [\text{g}/\text{cm}^2]$. However, the exact relationship to $\delta\rho R$ requires a model of the source and scattering material geometry. Nevertheless, the data clearly indicate significant variations in Y/Y_{avg} and, therefore, shell ρR anisotropies (blue areas are high ρR , and red low ρR). The data show a large ρR asymmetry aligned along the equator ($\theta \sim 90^\circ$) with a high ρR region near $\phi \sim 180^\circ$ and a low ρR around $\phi \sim 0^\circ$. The hot spot velocity is determined using neutron time-of-flight (nTOF) measurements of the Doppler-shifted DT neutron spectrum [10] (also indicated in Fig. 4), and closely aligns with the low- ρR region consistent with the observations of Rinderknecht *et al.* [45]. The direction of the radiation drive asymmetry including the impact of diagnostic

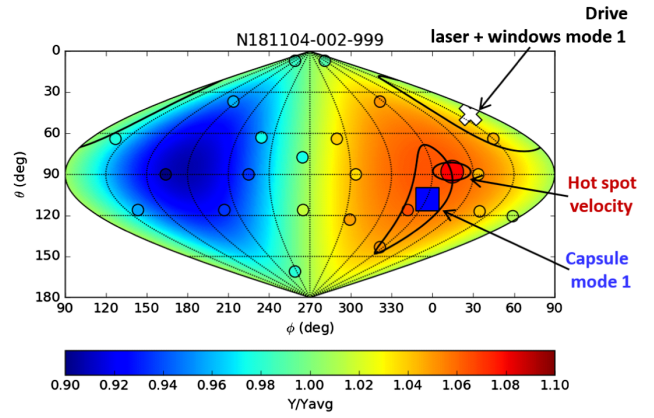


FIG. 4. RTNAD activation data for shot N181104 showing a significant asymmetry aligned principally toward $\sim 90-0$. Also shown is the hot spot velocity (circle) that aligns with the RTNAD data. The drive + window asymmetry (plus indicates the direction of less intense drive) and capsule (square indicates the direction of the thicker side) mode-1 asymmetries are also shown. The capsule asymmetry most closely aligns with the observed implosion asymmetry in this experiment.

windows and delivered laser energy balance calculated using a 3D view factor model [14] is also indicated Fig. 4. The drive asymmetry cannot fully explain the direction and magnitude of the observed asymmetry for N181104. However, the direction of the observed preshot HDC shell asymmetry mode 1, described in Figs. 1(d) and 1(e), aligns closely with the direction of the ρR asymmetries observed at peak compression as indicated in Fig. 4, strongly suggesting a linkage.

To determine if the magnitude of the HDC shell asymmetry correlates with the observed hot spot velocity with a larger dataset of recent experiments, the known radiation drive asymmetry [14] from peak laser power fluctuations and diagnostic window losses is estimated and then removed from the hot spot velocity vector [46], assuming that the relationship to the seeds remain linear [47]. The magnitude of that residual, or unexplained, hot spot velocity is compared to the magnitude of the HDC shell asymmetry [48] in Fig. 5. The residual hot spot velocity of N181104 is 92 km/s and with an amplitude of 0.78%, consistent with the overall observed trend in the broader dataset. This dataset also shows that the total hot spot velocity is correlated with the apparent ρR asymmetry determined from the RTNAD instrument suite, similar to earlier datasets [45]. Additionally, the RTNAD inferred asymmetry and asymmetry in the observed DSR measurements with the neutron spectrometer suite [8,10] are also correlated. The inferred ion temperature width from the Doppler-broadened DT neutron spectrum suggests higher-order flows induced by mode-1 asymmetries [12,49], and work is ongoing to compare these measurements to the hot spot velocity including a newly installed nTOF line of sight. Notably, this dataset shows considerable hot spot

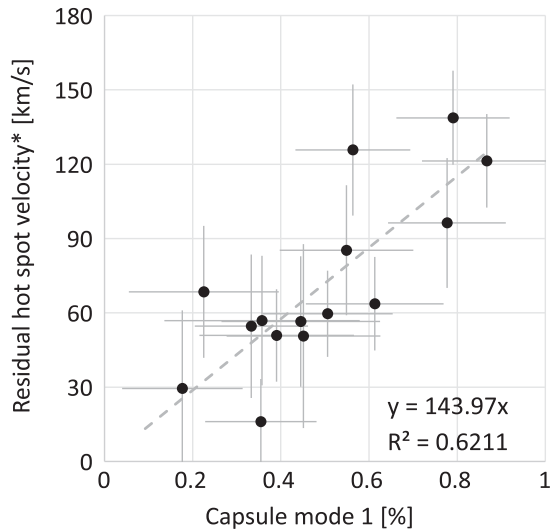


FIG. 5. Residual hot spot velocity (defined as the measured velocity vector with known seeds from radiation drive asymmetries [14] subtracted) for recent HDC experiments from HyB [27,50,51], HyE [52], and I-raum campaigns [24].

velocity sensitivity to the capsule mode-1 asymmetry 140 ± 30 km/s/%, and a large fraction of the experiments in this particular dataset seem to be impacted by this important new seed. The sensitivity determined from the data in Fig. 5 is consistent with the simulations in Fig. 3 when considering the spread in the data. The spread in the data is due to known sensitivities [6] of the hot spot velocity to platform parameters like v_{imp} and DSR that are varying in this dataset, measurement uncertainties, and the non-linearity of the hot spot velocity to high initial seeds [41]. It is thought that the introduction and growth of low-mode HDC thickness asymmetries occur in either the coating or polishing phases of capsule manufacture. The high empirically determined sensitivity motivates significant efforts to understand and mitigate.

It should be emphasized that the potential impact of a shell-induced asymmetry on the performance of an implosion is a strong function of the importance of alpha particle self-heating and the proximity to ignition. As noted earlier, an ~ 100 km/s hot spot velocity is expected to have a significant reduction ($\sim 38\%$) in total yield for an implosion that would have produced about $\sim 2 \times 10^{16}$ and 3% DSR, otherwise. However, a similar analysis predicts that impact would be catastrophic for an implosion that might otherwise produce 2×10^{17} total yield, instead suffering an $\sim 10\times$ reduction from a similar initial perturbation. In other words, perturbations on the order of those observed in Fig. 5 could reduce a potential approximately megajoule-class implosion to ~ 100 kJ of fusion yield. Therefore, this work places stringent new requirements on the capsule thickness symmetry that must become even more restrictive if implosion performances are to be improved significantly beyond the best implosions to date. Furthermore,

improvements in metrology to measure thickness uniformity may be needed. To that end, the development of optical and infrared interferometry techniques is underway, and early results are encouraging.

In summary, ablator shell-thickness nonuniformities have been revealed as a significant cause for 3D asymmetries in HDC-ablator implosion experiments at the NIF. This finding, while specific to HDC experiments, is likely applicable to all ablator (HDC, CH, Be, etc.) designs. However, the potential impact may vary due to the ability to manufacture sufficiently symmetric shells relative to the total shell thickness and the capability to metrologize as-built shells to required accuracy. Additionally, this newly identified seed has significantly perturbed recent implosions. To mitigate this issue, ongoing improvements in metrology will help identify problematic capsules earlier in the target fabrication process so that they can be excluded, and work is currently underway to determine and alleviate the root cause. Along with the sources of radiation drive asymmetries that have also recently been identified [14], we can now explain a significant majority of the hot spot velocities and ρR asymmetries observed in HDC ICF experiments at the NIF and are working to mitigate their sources.

The authors sincerely thank the NIF operations staff who supported this work. This work was performed under the auspices of the U.S. Department of Energy by Lawrence Livermore National Laboratory under Contract No. DE-AC52-07NA27344 and General Atomics under Contract No. DE-NA0001808.

-
- [1] E. I. Moses, *J. Phys. Conf. Ser.* **112**, 012003 (2008).
 - [2] J. D. Lindl, P. Amendt, R. L. Berger, S. G. Glendinning, S. H. Glenzer, S. W. Haan, R. L. Kauffman, O. L. Landen, and L. J. Suter, *Phys. Plasmas* **11**, 339 (2004).
 - [3] S. Atzeni and J. Meyer-ter-Vehn, *The Physics of Inertial Fusion*, International Series of Monographs on Physics (Oxford University Press, Oxford, 2004).
 - [4] J. P. Freidberg, *Plasma Physics and Fusion Energy* (Cambridge University Press, Cambridge, England, 2007).
 - [5] R. Betti, P. Y. Chang, B. K. Spears, K. S. Anderson, J. Edwards, M. Fatenejad, J. D. Lindl, R. L. McCrory, R. Nora, and D. Shvarts, *Phys. Plasmas* **17**, 058102 (2010).
 - [6] O. A. Hurricane *et al.*, *Phys. Plasmas* **27**, 062704 (2020).
 - [7] B. K. Spears *et al.*, *Phys. Plasmas* **19**, 056316 (2012).
 - [8] M. G. Johnson *et al.*, *Rev. Sci. Instrum.* **83**, 10D308 (2012).
 - [9] J. A. Frenje *et al.*, *Phys. Plasmas* **17**, 056311 (2010).
 - [10] R. Hatarik *et al.*, *J. Appl. Phys.* **118**, 184502 (2015).
 - [11] D. Eder *et al.*, *J. Phys. Conf. Ser.* **717**, 012014 (2016).
 - [12] D. Schlossberg *et al.*, *Phys. Rev. Lett.* (to be published).
 - [13] R. Tommasini *et al.*, *Phys. Rev. Lett.* **125**, 155003 (2020).
 - [14] B. J. MacGowan, HEDP (to be published).
 - [15] D. D. Ho, *Bull. Am. Phys. Soc.* **52**, 273 (2007);
 - [16] A. J. MacKinnon *et al.*, *Phys. Plasmas* **21**, 056318 (2014).

- [17] J. S. Ross, D. Ho, J. Milovich, T. Doppner, J. McNaney *et al.*, *Phys. Rev. E* **91**, 021101(R) (2015).
- [18] L. F. Berzak Hopkins *et al.*, *Phys. Rev. Lett.* **114**, 175001 (2015).
- [19] D. D. M. Ho, S. W. Haan, J. D. Salmonson, D. S. Clark, J. D. Lindl, J. L. Milovich, C. A. Thomas, L. F. B. Hopkins, and N. B. Meezan, *J. Phys. Conf. Ser.* **717**, 012023 (2016).
- [20] N. B. Meezan *et al.*, *Phys. Plasmas* **22**, 062703 (2015).
- [21] L. Divol *et al.*, *Phys. Plasmas* **24**, 056309 (2017).
- [22] L. F. Berzak Hopkins *et al.*, *Phys. Plasmas* **22**, 056318 (2015).
- [23] A. L. Kritcher *et al.*, *Phys. Plasmas* **25**, 056309 (2018).
- [24] H. F. Robey, L. Berzak Hopkins, J. L. Milovich, and N. B. Meezan, *Phys. Plasmas* **25**, 012711 (2018).
- [25] D. T. Casey *et al.*, *Phys. Plasmas* **25**, 056308 (2018).
- [26] K. L. Baker, C. A. Thomas, D. T. Casey, S. Khan, B. K. Spears *et al.*, *Phys. Rev. Lett.* **121**, 135001 (2018).
- [27] A. L. Kritcher *et al.*, *Phys. Plasmas* **27**, 052710 (2020).
- [28] D. S. Clark *et al.*, *Phys. Plasmas* **21**, 112705 (2014).
- [29] C. Young *et al.*, *Phys. Plasmas* **27**, 082702 (2020).
- [30] R. C. Shah, B. M. Haines, F. J. Wysocki, J. F. Benage, J. A. Fooks *et al.*, *Phys. Rev. Lett.* **118**, 135001 (2017).
- [31] D. T. Michel, I. V. Igumenshchev, A. K. Davis, D. H. Edgell, D. H. Froula, D. W. Jacobs-Perkins, V. N. Goncharov, S. P. Regan, A. Shvydky, and E. M. Campbell, *Phys. Rev. Lett.* **120**, 125001 (2018).
- [32] H. Huang, R. B. Stephens, S. A. Eddinger, J. Gunther, A. Nikroo, K. C. Chen, and H. W. Xu, *Fusion Sci. Technol.* **49**, 650 (2006).
- [33] H. Huang, B. J. Kozioziemski, R. B. Stephens, A. Nikroo, S. A. Eddinger, K. C. Chen, H. W. Xu, and K. A. Moreno, *Fusion Sci. Technol.* **51**, 519 (2007).
- [34] B. J. Kozioziemski, J. A. Koch, A. Barty, H. E. Martz Jr., W.-K. Lee, and K. Fezzaa, *J. Appl. Phys.* **97**, 063103 (2005).
- [35] B. J. Kozioziemski, J. D. Sater, J. D. Moody, J. J. Sanchez, R. A. London, A. Barty, H. E. Martz, and D. S. Montgomery, *J. Appl. Phys.* **98**, 103105 (2005).
- [36] T. Parham *et al.*, *Fusion Sci. Technol.* **69**, 407 (2016).
- [37] A single projection view from a contact radiograph of this shell showed a mode-1 amplitude of $0.55 \pm 0.2\%$. Because the contact radiograph is from a single projection, these values cannot be compared directly. However, using a statistical argument of randomly aligned and projected mode-1 values onto a single view, the single view is most likely to be 79% of the total amplitude, and so we can infer a range of values within a typical 1 sigma error of $0.7 + 0.6/ - 0.2\%$ (including the diagnostic uncertainty). The agreement between the two approaches gives confidence in the fidelity of this challenging measurement.
- [38] M. M. Marinak, G. D. Kerbel, N. A. Gentile, O. Jones, D. Munro, S. Pollaine, T. R. Dittrich, and S. W. Haan, *Phys. Plasmas* **8**, 2275 (2001).
- [39] C. R. Weber *et al.*, *Phys. Plasmas* **27**, 032703 (2020).
- [40] The slight offset at the center (hot spot velocity at zero m1 asymmetry) is due to the inclusion of other perturbations in the capsule (including a surrogate model for the fill tube) and drive in this postshot simulation and numerical error.
- [41] B. K. Spears *et al.*, *Phys. Plasmas* **21**, 042702 (2014).
- [42] O. A. Hurricane *et al.*, *Phys. Plasmas* **24**, 092706 (2017).
- [43] S. P. Hatchett, Report No. UCRL-JC-108348, Lawrence Livermore National Laboratory, Livermore, CA, 1991).
- [44] C. B. Yeaman and D. L. Bleuel, *Fusion Sci. Technol.* **72**, 120 (2017).
- [45] H. G. Rinderknecht, D. T. Casey, R. Hatarik, R. M. Bionta, B. J. MacGowan, P. Patel, O. L. Landen, E. P. Hartouni, and O. A. Hurricane, *Phys. Rev. Lett.* **124**, 145002 (2020).
- [46] $\langle x, y, z \rangle$ in units of km/s through the determined sensitivity of drive to hot spot velocity.
- [47] The hot spot velocity to seed relationship becomes nonlinear around ~ 100 km/s as is evident in Fig. 3. While some nonlinear behavior may be present in the dataset, only two absolute hot spot velocities > 100 km/s, and so we expect this to play a minor role, possibly contributing some noise to the hot spot to shell asymmetry sensitivity.
- [48] The capsule mode-1 value does not include a 5% contribution in the denominator (mode 1) for DT fuel mass or any mode-1 thickness variation in the DT fuel, which is typically $< 1\%$ and so usually insignificant.
- [49] T. J. Murphy, *Phys. Plasmas* **21**, 072701 (2014).
- [50] A. B. Zylstra *et al.*, *Phys. Plasmas* **27**, 092709 (2020).
- [51] Hohenberger *et al.*, *Phys. Plasmas* **27**, 112704 (2020).
- [52] Zylstra *et al.*, *Phys. Rev. Lett.* (to be published).